Biochimica et Biophysica Acta 1847 (2015) 314–327

Contents lists available at ScienceDirect

Biochimica et Biophysica Acta

journal homepage: www.elsevier.com/locate/bbabio

Monte Carlo simulations of excitation and electron transfer in grana membranes

Krzysztof Gibasiewicz [a,*], Małgorzata Adamiec [b], Robert Luciński [b], Wojciech Giera [a], Przemysław Chełminiak [a], Sebastian Szewczyk [a], Weronika Sipińska [a], Edyta Głów [a], Jerzy Karolczak [a,c], Rienk van Grondelle [d], Grzegorz Jackowski [b]

[a] Department of Molecular Biophysics, Faculty of Physics, Adam Mickiewicz University, ul. Umultowska 85, 61-614 Poznań, Poland
[b] Department of Plant Physiology, Institute of Experimental Biology, Faculty of Biology, Adam Mickiewicz University, ul. Umultowska 89, 61-614 Poznań, Poland
[c] Ultrafast Laser Spectroscopy Center, Faculty of Physics, Adam Mickiewicz University, ul. Umultowska 85, 61-614 Poznań, Poland
[d] Department of Physics and Astronomy, VU University, De Boelelaan 1081, 1081 HV Amsterdam, The Netherlands

ARTICLE INFO

Article history:
Received 21 July 2014
Received in revised form 5 December 2014
Accepted 9 December 2014
Available online 15 December 2014

Keywords:
Photosystem II
Light Harvesting Complex II
Excitation energy transfer
Electron transfer
Streak camera
Monte Carlo simulation

ABSTRACT

Time-resolved fluorescence measurements on grana membranes with instrumental response function of 3 ps reveal faster excitation dynamics (120 ps) than those reported previously. A possible reason for the faster decay may be a relatively low amount of "extra" LHCII trimers per reaction center of Photosystem II. Monte Carlo modeling of excitation dynamics in $C_2S_2M_2$ form of PSII–LHCII supercomplexes has been performed using a coarse grained model of this complex, constituting a large majority of proteins in grana membranes. The main factor responsible for the fast fluorescence decay reported in this work was the deep trap constituted by the primary charge separated state in the reaction center (950–1090 cm^{-1}). This value is critical for a good fit, whereas typical hopping times between antenna polypeptides (from ~4.5 to ~10.5 ps) and reversible primary charge separation times (from ~4 to ~1.5 ps, respectively) are less critical. Consequently, respective mean migration times of excitation from anywhere in the PSII–LHCII supercomplexes to reaction center range from ~30 to ~80 ps. Thus 1/4–2/3 of the ~120-ps average excitation lifetime is necessary for the diffusion of excitation to reaction center, whereas the remaining time is due to the bottle-neck effect of the trap. Removal of 27% of the Lhcb6 apoprotein pool by mutagenesis of *DEG5* gene caused the acceleration of the excitation decay from ~120 to ~100 ps. This effect may be due to the detachment of LHCII-M trimers from PSII–LHCII supercomplexes, accompanied by deepening of the reaction center trap.

1. Introduction

In grana membranes, Photosystem II occurs as a dimeric PSII–LHCII supercomplex composed of two core complexes (C_2) and two sets of symmetrical, peripheral antenna complexes surrounding the cores. Each core complex contains one reaction center and inner light-harvesting complexes CP43 and CP47 (comprising PsbB and PsbC apoproteins, respectively). The set of peripheral antenna complexes makes CP29, CP26 and CP24 which are connected directly to the core as well as two types of LHCII trimers: S trimers (strongly bound to the core, in contact with CP43 and CP26) and M trimers (moderately bound to the core, in contact with CP29 and CP24) [1]. Presumably, the largest supercomplex called $C_2S_2M_2$ – containing two LHCII S trimers and two M trimers – is the complex which is the most abundant one in *Arabidopsis thaliana* thylakoid membranes [2].

The antenna size of PSII–LHCII supercomplex plays an important role in excitation energy transfer within this complex. Namely, studies performed on PSII–LHCII supercomplexes with various antenna sizes (purified from grana membranes by separation on sucrose gradients) demonstrated that a decrease in size of the complex led to speeding up of fluorescence kinetics [3]. However, since purification of PSII–LHCII supercomplexes with different antenna sizes requires the application of detergents to solubilize thylakoid membranes, which may affect adversely the architecture and excitation energy transfer of the supercomplexes, native membranes (grana or thylakoids) remain a preferable system to study excitation energy transfer in PSII. In the case of thylakoids, however, contribution from Photosystem I makes interpretation of the experimental data of excitation energy transfer in PSII much more complex and problematic [4].

Using single photon counting approach it was shown that the average excitation lifetime in grana is about 150 ps [3,5,6], significantly less than the values reported in older papers [7,8] which came likely from

Abbreviations: FWHM, full width at half maximum; IRF, instrumental response function; MC, Monte Carlo; Hepes, (4-(2-hydroxyethyl)-1-piperazineethanesulfonic acid); PVDF, polyvinylidene difluoride; RC, reaction center

* Corresponding author. Tel.: +48 61 8296370.
E-mail address: krzyszgi@amu.edu.pl (K. Gibasiewicz).

http://dx.doi.org/10.1016/j.bbabio.2014.12.004
0005-2728/

grana samples "contaminated" by closed complexes (with reduced Q_A acceptor) or from uncoupled LHCII trimers. In principle in any studies performed on grana membranes with the use of fluorescence techniques there is some uncertainty associated with the presence of regions rich in "extra" LHCII trimers [9]. Precise determination of the number of LHCII trimers per PSII core may be helpful in the modeling of excitation energy transfer in native photosynthetic membranes. Recently, a coarse-grained model was successfully introduced allowing calculation of a few basic parameters influencing the excitation decay in PSII–LHCII supercomplexes and depicting interpolypeptide excitation hopping, primary and secondary charge separation, and charge recombination in PSII reaction centers [3,5,6]. These parameters allow estimation of mean migration time of excitation from the antenna system to reaction center and, in consequence, allow conclusions on the limiting steps in excitation decay.

In this paper we report significantly faster excitation decay in grana membranes than previously reported and model this decay using the Monte Carlo method of excitation and electron transfer in PSII–LHCII supercomplex. A model of significant reversibility of primary charge separation is supported and a new set of hopping and electron transfer parameters is proposed to be consistent with a short, 120-ps, average excitation lifetime. The data obtained for WT preparations are confronted with those recorded for mutant lacking ~25% of Lhcb6 apoprotein pool (CP24 complex).

2. Materials and methods

2.1. Plant material and growth conditions

A. thaliana plants (ecotype Columbia) were grown for five weeks in 42-mm Jiffy peat pellets on sphagnum peat moss and wood pulp (AgroWit, Przylep, Poland) under long-day conditions (16 h/8 h, light/dark) with an irradiance of 110 μmol photons m^{-2} s^{-1} at a constant temperature of 22 °C and 70% humidity. *A. thaliana* seeds (SALK_099162) with a T-DNA insertion in the *DEG5* gene (At4g18370) were obtained from NASC (Nottingham Arabidopsis Stock Center, Nottingham, UK). The T-DNA insertion was confirmed and hetero/homozygosity was analyzed by PCR using the following primers: forward, 5′-GCTTTTTCCTCA ATCTTCAATAC-3′ and reverse, 5′-AGGATTTAGTTCACGTCCCTC-3′ for the Deg5 sequence, and LBb1 (5′-GCGTGGACCGCTTGCTGCAACT-3′) for the insertion.

2.2. Isolation of thylakoids and grana membranes (BBY samples)

Intact chloroplasts were prepared using the Sigma Chloroplast Isolation Kit (Sigma-Aldrich, St. Louis, MO, USA) as described by us earlier [10] and the isolation of thylakoids was done according to [11]. Grana membranes were isolated from chloroplasts of wild type (WT) or *deg5* mutant plants according to the method of [12] with the modifications described by [13], using Triton X-100/Chl ratio of 21.2:1 (v/v) to solubilize thylakoid membranes. The pellet of grana membranes was resuspended in a small volume of a buffer containing 20 mM Hepes/KOH (pH = 7.5), 5 mM $MgCl_2$, 15 mM NaCl and 10% glycerol and stored at −20 °C.

2.3. SDS-PAGE, immunoblotting, protein quantitation and calculation of the number of LHCII trimers per PSII core

SDS-PAGE of thylakoids or grana membranes was performed in 14.5% acrylamide gels using the [14] buffer system. The gels were stained with 0.025% CBB G-250 by the method of [14]. The stained gels were scanned using Gelix One software (Biostep, Jahnsdorf, Germany) and the number of LHCII trimers per PSII core was calculated as [(Lhcb1 + Lhcb2 + Lhcb3) / Lhcb4] / 3. A 1.1 times stronger binding of CBB G-250 to Lhcb4 vs Lhcb1/2/3 was taken into account [15].

To identify and quantify selected PSII apoproteins electrophoretically resolved thylakoid and grana membranes were electrotransferred onto PVDF membranes (Roche, Basel, Switzerland), reacted with polyclonal antibodies raised against Lhcb1–6, PsaB, PsbC or PsbD apoproteins (Agrisera, Vannas, Sweden), detected by applying goat anti-rabbit biotinylated immunoglobulin G (Agrisera, Vannas, Sweden) and visualized by using the Enhanced Chemiluminescence System (ECL) according to the manufacturer's recommendations (Lumi-Light Western Blot Substrate, Roche Diagnostics GmbH, Mannheim, Germany). The quantification of immunostained signals was performed using Gelix One software.

2.4. Chlorophyll quantitation

The Chl concentration was assayed according to [16].

2.5. Measurements with streak camera

For streak camera measurements, 20 μl of concentrated grana membranes solution was diluted (to final OD of ~0.1 cm^{-1} at maximum of Q_y band) in 2 ml 20 mM Hepes buffer pH = 6.5 containing 15 mM NaCl, 5 mM $MgCl_2$, 0.005% β-dodecylmaltoside, and fresh 1 mM $K_3Fe(CN)_6$ in order to keep the reaction center in open state. The small amount of detergent was added in order to minimize formation of large aggregates of grana membranes.

The time-resolved fluorescence measurements were performed using the setup in Laser Centrum, Vrije Universiteit, Amsterdam described in detail elsewhere [17]. The samples were excited at 400 nm with a repetition rate of 125 kHz by vertically polarized ~100-fs pulses. The diameter of the laser spot on the sample was of about 200 μm. The typical energy of excitation was ~1 nJ per pulse, well below the level leading to annihilation.

The fluorescence signal, measured at a right angle with respect to the excitation beam by the detection system composed of spectrograph (Chromex 250IS), streak camera (Hamamatsu C5680), and CCD camera (Hamamatsu C4880), was recorded in three time windows: ~150 ps, ~350 ps, and ~1500 ps with temporal resolution (FWHM of instrument response function) of ~3 ps, ~6 ps, and ~16 ps, respectively. In order to obtain good enough signal to noise ratio, the fluorescence signal was accumulated for 4× (10–20 min), 4× (5–10 min), and 4× (1–4 min) in the respective time windows. The sample was placed in a rotating cuvette to ensure that each laser pulse illuminated a fully relaxed sample. The rotating cuvette was tilted at ~45° relative to excitation beam and the optical pathway length in the sample was ~2 mm.

The time resolved fluorescence spectra collected in the range 600–770 nm in all three time windows were analyzed simultaneously and globally using the GLOTARAN software [18] yielding decay associated spectra (DAS) [19].

2.6. Time-correlated single photon counting measurements

Time-correlated single photon counting (TC-SPC) measurements were performed at the Center for Ultrafast Laser Spectroscopy, Adam Mickiewicz University, Poznań, using the setup described elsewhere [20–22]. Grana membrane samples were suspended in a similar medium as in the case of streak camera-based measurements. The concentrated sample was diluted in a buffer of pH = 7.5 and of similar composition to that one used for the streak camera measurements. Fluorescence kinetics were recorded by thermoelectrically cooled MCP-PMT R3809U-05 (Hamamatsu), following excitation at 400 nm by 2-ps laser pulses of typical energy of 1 pJ per pulse at a repetition rate of 4 MHz. The sample was placed in a quartz fluorescence cuvette (1 cm × 1 cm) and stirred with a small magnetic stirrer during the measurements.

Fluorescence kinetics were recorded in a 2.5 ns time window with a resolution of 0.61 ps per channel (4096 channels) at 680 nm and

analyzed by software using delta function convolution method [23] and simplex procedure [22]. According to the delta function convolution method, fluorescence decays were fitted by convolution of the term containing three-exponential functions with the reference function measured as fluorescence decay of pinacyanol solution in methanol at 680 nm [23]. The decay of pinacyanol solution was characterized by 8–10-ps lifetime. Instrument response function (IRF) was measured also at 400 nm using light scattered in Ludox solution and was typically of 42 ps FWHM. IRF was measured in this way only in order to compare its width (FWHM) with the IRF width reported in other papers, and it was not used in the fitting procedure since the quality of fits was better when using pinacyanol decay as a reference.

3. Results and discussion

3.1. Biochemical properties of grana membranes of WT and deg5 mutant plants

To study excitation dynamics in PSII–LHCII supercomplexes, grana membranes of the WT and *deg5* plants were analyzed. The mutants, derived from source SALK_099162 line were earlier shown to be homozygous for *T-DNA* insertion in the 2nd exon of At4g18370 gene, 429 bp downstream of ATG codon and complementable by introduction of a wild-type copy of the gene [11,24]. To assess accurately the purity of the grana membranes in terms of pigments composition, PSI/PSII ratio was calculated as the total number of Chl $a + b$ molecules associated with a PSI complex per the total number of Chl $a + b$ molecules associated with PSII complex in the samples. To perform the calculation it was necessary to determine Chl *a*:Chl *b* ratio and the number of LHCII trimers per PSII core of the grana membranes. The determined Chl *a*:Chl *b* ratio was 2.13:1 and 2.14:1 for WT plants and the mutants, respectively. Lhcb1–4 levels were quantified by image analysis of CBB G-250 stained gels to estimate a number of LHCII trimers per PSII core (Fig. 1). In WT plants and *deg5* mutants there were on average 2.18 ± 0.01 and 2.14 ± 0.01 LHCII trimers per PSII core, respectively (and a double amount per PSII core dimer). Chl *a*:Chl *b* ratios and numbers of LHCII trimers per PSII core were used to calculate PSI/PSII ratio, which independently of exact number of Chls *a* in PSII–LHCII supercomplex was 0.01 or less (see Table A1 in Appendix A for numbers of considered Chls *a* and for formulas used for calculations). In agreement with the results of determination of PSI/PSII ratio it was found that grana membranes isolated both from chloroplasts of WT plants and *deg5* mutants completely lacked PsaB apoprotein (PSI core) (Fig. 2). Thus, no matter which Chl *a*/P680 stoichiometry is correct, grana membranes used in this study were found to be sufficiently pure (both in terms of pigment as well as protein composition) to avoid including PSI contribution to the fit results.

Immunoblot-based analysis was performed to study the content of Lhcb1–6 apoproteins in grana membranes. Equal amount of PsbC apoprotein (a PSII core protein) was used to normalize the signals detected by anti-Lhcb1–6 antibodies. Supplemental Fig. 1 presents the results of the verification of grana membranes chlorophyll quantity/immunological signal linearity range for Lhcb1–6 and PsbC apoproteins whereas the outcome of the immunotitration is displayed as Fig. 3. It was established that while the amount of Lhcb1–5 apoproteins per PSII core in the mutant equaled the values found for WT plants the accumulation pattern of Lhcb6 was different — *deg5* grana membranes lacked 27% of the pool present in the wild type.

PSII–LHCII supercomplex called $C_2S_2M_2$ is considered to be by far the most abundant complex present in *A. thaliana* grana membranes as judged by the similarity of average excited-state lifetime of purified $C_2S_2M_2$ complexes to this determined for grana membranes [3,6]. Taking into account that there are 4 LHCII trimers per PSII core dimer in the $C_2S_2M_2$ particle then there are 0.36 and 0.28 trimers of "extra LHCII" per PSII core dimer in WT and *deg5* grana membranes, respectively. CP24 is thought to play an important role in determining the organization of PSII–LHCII supercomplex by linking LHCII-M trimers to PSII core since grana membranes of koCP24 mutants exhibited C_2S_2 arrays interspersed by "extra" LHCII-rich patches formed by LHCII M trimers which segregated away from $C_2S_2M_2$ complexes due to the loss of Lhcb6 apoprotein [25,26]. Considering that *deg5* mutant lacks as little as about 27% of the Lhcb6 pool found to be present in wild type plants it can be assumed that the mutant lacks about 27% of its LHCII-M trimers as well. Thus roughly either about 25% of the supercomplexes is present as C_2S_2 (lacking both CP24 copies and both LHCII-M trimers) or about 50% of the supercomplexes are represented by C_2S_2M form (lacking a single CP24 copy and a single LHCII-M trimer) thus a content of PSII-bound LHCII trimers is reduced to 3.5 per core dimer. This inevitably leads to an enlargement of "extra" LHCII pool by 0.5 LHCII M trimers per PSII core dimer i.e. on average there are about 0.78 "extra LHCII" trimers (M) per PSII core dimer in *deg5* plants. Segregation of LHCII-S trimers away from mutant $C_2S_2M_2$ complexes, in turn, seems to be extremely improbable since supposedly arising C_2M assemblies would lose Lhcb5 apoproteins along with LHCII S trimers [3] and this is in disagreement with our finding that Lhcb5 contents per PSII core in WT and *deg5* plants were equal (Fig. 3). It is not clear why *deg5* mutants are deficient in Lhcb6 apoprotein but it may tentatively be suggested that

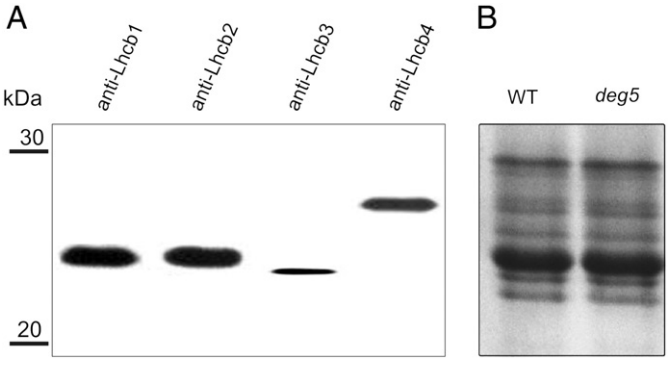

Fig. 1. Identification and quantification of the number of LHCII trimers per PSII core. Analyses were conducted on grana membranes isolated from leaves of wild type plants (WT) and *deg5* mutants. (a) Identification of Lhcb1–4 apoproteins. Grana membranes isolated from leaves of wild type plants (WT) were resolved by SDS-PAGE, electrotransferred onto PVDF membranes and the membranes were immunostained with relevant antibodies. (b) Quantification of the number of LHCII trimers per PSII core. Grana membrane samples isolated from leaves of wild type (WT) and *deg5* plants were resolved by SDS-PAGE (on the basis of an equal amount of chlorophyll), stained by CBB G-250 and the gels scanned. The number of LHCII trimers per PSII core was calculated as [(Lhcb1 + Lhcb2 + Lhcb3) / Lhcb4] / 3. A 1.1 times stronger binding of CBB G-250 to Lhcb4 vs Lhcb1/2/3 was taken into account.

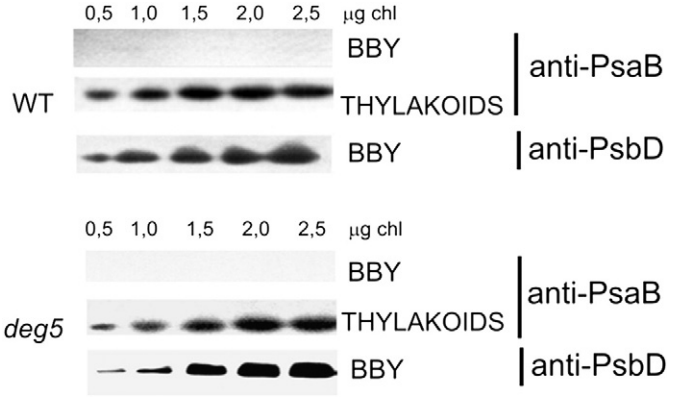

Fig. 2. Analysis of the content of PsbD (PSII core) and PsaB (PSI core) apoproteins in thylakoids and grana membranes isolated from leaves of wild type plants (WT) and *deg5* mutants. Thylakoids and grana membranes isolated from leaves of wild type plants (WT) and *deg5* mutants were resolved by SDS-PAGE, electrotransferred onto PVDF membranes and the membranes were immunostained with relevant antibodies. The samples were loaded at five different chlorophyll amounts.

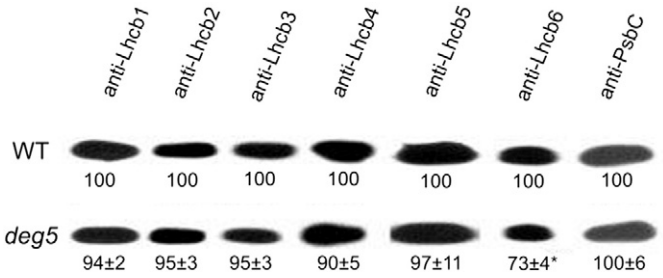

Fig. 3. Quantification of the steady-state level of Lhcb1–6 and PsbC apoproteins in grana membranes isolated from leaves of wild type plants (WT) and *deg5* mutants. Grana membranes were resolved by SDS-PAGE (on the basis of an equal immunological signal of PsbC), electrotransferred onto PVDF membranes and the membranes were immunostained with relevant antibodies and scanned. Individual signals of Lhcb1–6 in mutant grana membrane samples were quantified relative to signals identified for BBY samples isolated from wild type plants (100%). The percentages are indicated under the corresponding lanes. The asterisks indicate the data for which wild type plant/mutant plant differences were significant ($P < 0.05$).

AtDeg5 is either directly involved in the control of Lhcb6 turnover or targets "real" Lhcb6-hydrolyzing protease.

3.2. Fluorescence decay in WT grana membranes

Fig. 4A presents typical results of global analysis of fluorescence time-resolved spectra measured with streak camera for WT grana membranes on excitation at 400 nm. The excitation pulses were kept at sufficiently low level to avoid singlet–singlet exciton annihilation (0.25 nJ; it was tested that the kinetics starts to accelerate, most likely due to singlet–singlet exciton annihilation, only when the pulse energy is increased to above ~5–10 nJ). The two spectral components, determined in the case of data shown in Fig. 1A to be 47 ps and 165 ps, are attributed to two phases of excitation quenching by two-step charge separation in reaction center, the first step being reversible and the next one — irreversible. Consequently, the first phase of fluorescence decay originates from partial decay of excited states caused by a formation of equilibrium between exited states in antenna and primary charge separated (dark) state in RC, whereas the second phase originates from decay of this equilibrated excited state by the secondary step of charge separation.

It should be noted that the fluorescence decay in grana membranes, when measured by TC-SPC technique, has been usually described by three subnanosecond components (Table 1) including our own measurements (see below and Table 1). Resolution of only two components in our streak camera measurements may be a result of poorer signal to noise ratio of the experimental traces relative to the data collected when using the TC-SPC method.

Although both spectra peak at 682 nm, the slower component is slightly red-shifted and broader towards red with respect to the faster component (FWHM of ~13 nm for the 165-ps DAS and FWHM of ~9 nm for the 47-ps DAS). Moreover, the spectrum of the faster component shows characteristic valley at around 710 nm, which is absent from the slower component. These features reveal a contribution of excitation energy transfer from "blue" to "red" chlorophylls occurring on the time scale of the fast component. In order to make this contribution visible more explicitly, the 47-ps DAS has been decomposed on two components: excitation decay spectrum of bulk chlorophylls *a* (the major one) and excitation energy transfer component (the minor one) which is conservative in shape (the areas of positive and negative parts of the spectrum are the same) (Fig. 4B). Then, the negative part of the "energy transfer spectrum" has been added to the 165-ps DAS yielding the corrected spectrum, ascribed to decay of bulk Chls *a* occurring on a slower, 165-ps time scale (Fig. 4B). The spectral shapes of both extracted pure excitation quenching of bulk Chls, the 47- and 165-ps

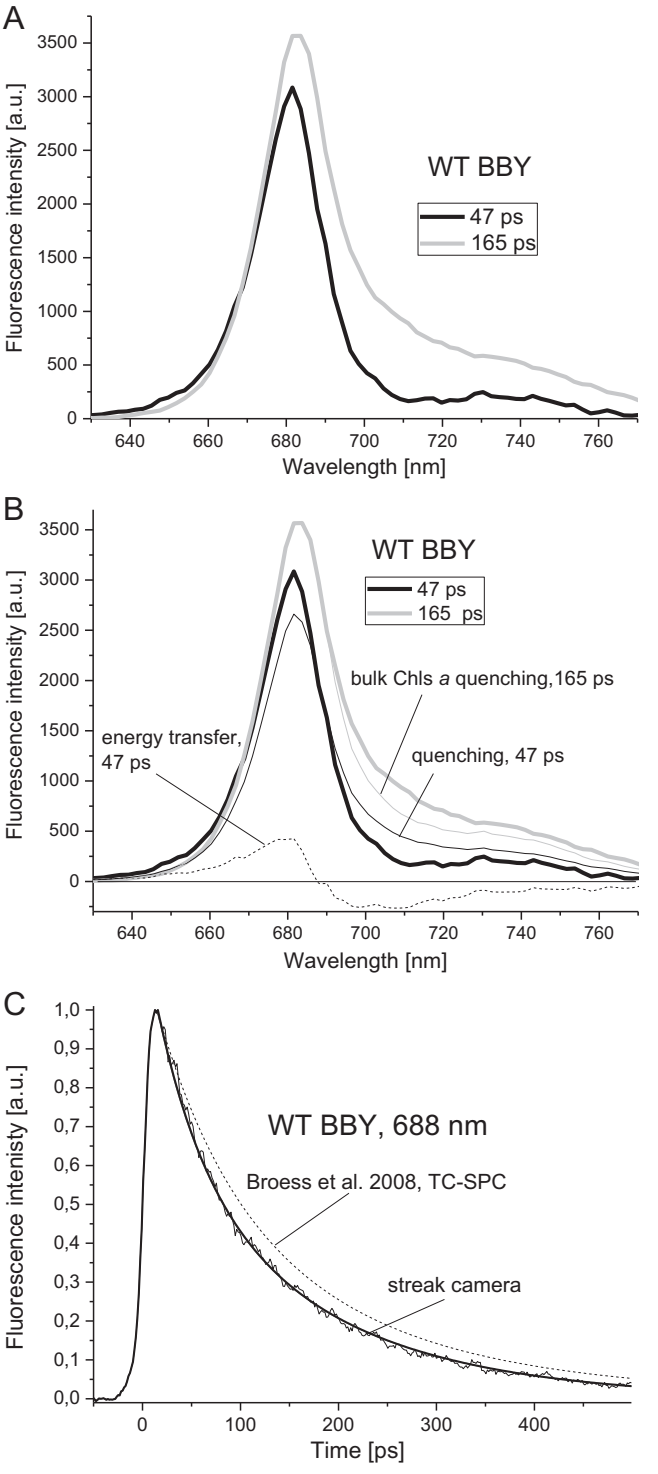

Fig. 4. Fluorescence decay associated spectra and fluorescence kinetics at 688 nm for WT grana membranes recorded on excitation at 400 nm. (A): decay associated spectra, (B): the fast decay associated spectrum (47 ps; thick solid black line) was decomposed on two components: the major one depicting the fast component of bulk chlorophyll quenching (thin solid black line) and the minor one depicting excitation energy transfer from high- to low-energy chlorophylls (thin dashed black line). The slow decay associated spectrum (165 ps; thick solid gray line) contains contributions from excitation quenching of both bulk and red-shifted Chls *a*. Calculated spectrum originating exclusively from bulk chlorophylls *a* quenching decaying in 165 ps was presented as a thin solid gray line. (C): fluorescence decay kinetics.

ones, are very similar to each other, as expected. The difference between "full" 165-ps spectrum and the corrected 165-ps spectrum is ascribed to decay (quenching) of excited red-shifted Chls.

Table 1
Fluorescence decay (detection at 680 and 688 nm) fitting results of grana membranes' samples reported by various authors using different experimental set-ups.

λ_{em} [nm]	Author	Technique	IRF[(2)] [ps]	FWHM[(3)] [ps]	τ_1 (A_1) [ps]	τ_2 (A_2) [ps]	τ_3 (A_3) [ps]	$\tau_{av}^{(4)}$ [ps]
688	**This work**	**Streak**	**3**	**83**	**47 (0.39)**	**165 (0.61)**	–	**119** ($n = 3$;119–125)
	[6][(1)]	TC-SPC	60	310	74 (0.417)	175 (0.510)	377 (0.071)	147
680	This work	streak	3	81	47 (0.47)	165 (0.53)	–	110 ($n = 3$;110–117)
	This work	TC-SPC	42	156	67 (0.664)	194 (0.316)	928 (0.020)	124 ($n = 4$;119–127)
	[5][(1)]	TC-SPC	60	330	80 (0.455)	212 (0.525)	633 (0.020)	160

Fluorescence decays were fitted by function: $\Sigma A_i \exp(-\tau_i/t)$, where $i = 2$ or 3, and $\Sigma A_i = 1$.
[(1)]The fit parameters were taken from [5] and [6]. The fourth component of ~2–3 ns of very small amplitude, <1%, was not shown and was neglected when calculating τ_{av}. [(2)]IRF — instrument response function. No information is available in [5] and [6] on how IRF was determined. In this work, IRF was determined as FWHM of scattered light collected after excitation pulse at 400 nm (TC-SPC) or white light (streak). [(3)]FWHM — full width at half maximum of time-resolved fluorescence decay signal measured at indicated λ_{em}. As an exception, FWHM was estimated from fluorescence signal collected at $\lambda_{em} = 693$ nm [5]. [(4)]In brackets, ranges of τ_{av} values are shown, obtained in n measurements performed by analyzing independent biological samples. In bold: parameters of the fluorescence decay curve simulated in the MC method.

These considerations allowed concluding that fluorescence quenching detected below and above 688 nm is "accelerated" and "decelerated", respectively, due to contribution from excitation energy transfer. Thus, it is fluorescence detected at 688 nm that may reflect pure excitation quenching in a proper way. For that reason most of the following considerations are based on the fluorescence kinetics measured at this wavelength.

It should be noticed that the difference in the spectral shapes of the two kinetic components (47 ps and 165 ps) was not reported in the previous studies using global analysis of fluorescence decay in PSII membranes and resolving similar components [5,27]. This might be due to the fact that the fastest kinetic component resolved by Broess et al. [5] was ~80 ps. Such a slow component could have been already dominated by fluorescence emitted by relaxed states equilibrated over the red-shifted chlorophylls. Probably this is also the reason why the two fluorescence decay associated spectra of 131 ps and 322 ps resolved in [27] were similar in shape. However, in [27] an extra 15-ps component was resolved clearly indicating excitation energy transfer from high to low energy chlorophylls. This observation reinforces attribution of the 47-ps component resolved in our studies to both excitation decay and energy equilibration process and justifies the different spectral shapes of the 47- and 165-ps spectra (Fig. 4A). Some spectral heterogeneity supporting the presence of excitation energy transfer in PSII membranes was also inferred from wavelength-dependent steady-state photochemical quenching studies [28,29].

It is understandable that our inability to resolve excitation decay and energy equilibration contributions as separate kinetic components in the fitting procedure does not mean that both of them are of exactly the same lifetime. It is likely that the equilibration lifetime is shorter and the decay lifetime is somewhat longer than 47 ps.

3.3. A comparison of fluorescence decay reported for WT grana membranes in this work with previous data

Fluorescence decay curve for WT grana membranes on excitation at 400 nm and detection at 688 nm, together with a fit (originating from a global analysis presented as Fig. 4A) and the fit curve reconstructed from the parameters of the fluorescence decay reported by [6] (excitation at 420 nm, detection at 688 nm, TC-SPC-based approach) are given in Fig. 4C. It can be seen that the latter decay is significantly slower than that one measured by us. This is also reflected by higher values of the respective lifetimes (Table 1). Relevant calculations led to the average fluorescence lifetimes of 147 ps [6] and 119 ps (this work). Similar average lifetimes of ~150 ps have been reported in a few other papers from the same group [3,5,6] and our value of ~120 ps has been confirmed in a few independent measurements (Table 1).

In order to explain the discrepancy between the fluorescence decay kinetics measured with TC-SPC [3,5] and by us with the streak camera (this work) we extensively studied fluorescence decay in WT grana membranes using also TC-SPC technique. Fitting results (for fluorescence emission detected at 680 nm) of the measurements performed by us with both streak camera set up and TC-SPC approach and by [6] with the application of TC-SPC approach are shown in Table 1.

Fit parameters originating from streak camera measurements at 680 nm come from the global analysis performed on the same experimental data as those analyzed for finding the parameters at 688-nm emission (Table 1). Therefore, the lifetimes, 47 and 165 ps, are the same at both wavelengths. As explained above, decay at 680 nm is somewhat faster than at 688 nm ($\tau_{av} = 110$ vs. 119 ps, Table 1) due to the contribution from excitation energy transfer to lower-energy chlorophylls. This effect is modeled by a set of different relative amplitudes than at 688 nm. When using the TC-SPC method, as many as three exponential components were resolved: 67, 194, and 928 ps, with the slowest component of small but significant contribution (0.02). These parameters are somewhat similar to those reported by [5] (80, 212, and 633 ps). However, together with relative amplitudes of particular components, the average fluorescence lifetime measured by [5] is again significantly longer, 160 ps, than the average lifetime calculated by us, 124 ps (Table 1).

In order to find the reason why the kinetics measured by us, using both streak camera and TC-SPC, are faster than those measured by [5,6] we compared instrumental response functions (IRF) used by us and in [5,6]. The width of the IRF in our TC-SPC setup was about 42 ps (Table 1), which is significantly smaller than the 60-ps IRF reported by [5,6]. Even more dramatic differences may be noted when directly comparing the width (FWHM) of fluorescence decay signals being an effect of convolution of IRF and multiexponential decay. It was ~160 ps in our TC-SPC measurements, and 310–330 ps in the case of the TC-SPC setup used by [5,6]. On the other hand, the authors of [5] presented the result of a control experiment performed with the use of the streak camera of ~3-ps resolution demonstrating similar (or in fact even slower) fluorescence decay to this measured by them using TC-SPC. Since our streak camera measurements were of similar ~3-ps resolution, we cannot attribute faster fluorescence decay measured by us to a better temporal resolution. However, the differences in the fluorescence kinetics measured by us using the two different techniques indicate that using TC-SPC technique alone may result in overestimation of the average fluorescence lifetime in PSII preparations.

In consequence the most plausible reason why fluorescence decay reported by [5,6] was slower than that reported in this work is that our grana samples contained less "extra" LHCII trimers per PSII–LHCII supercomplex (a total number of 2.18 LHCII trimers per PSII core vs 2.45 detected in spinach grana membranes by [5,6]). In vitro,

aggregation of purified LHCII trimers was shown to cause fluorescence decay to be considerably faster with respect to unaggregated trimers [30] thus it may be suggested that grana membranes samples studied by Broess et al. [5,6] were enriched in unaggregated form of "extra" LHCII trimers with respect to the samples studied in this work. Therefore it may be suggested that aggregation state of "extra" LHCII varies in a species-specific manner.

3.4. Monte Carlo simulations for WT grana membranes

Having found that the overall decay of excited states of PSII–LHCII supercomplexes was faster than that reported previously we determined independently a set of four molecular rate constants based on: 1) the fluorescence kinetics at 688 nm measured with streak camera and 2) a coarse-grained model of PSII. These rate constants are similarly defined as those reported by [3,5,6], and depict: 1) hopping between particular nodes (light harvesting complexes) in the polypeptide network (k_{hop}; to be accurate, this parameter is modulated by the numbers of Chls *a* in each node — see below), 2) primary (reversible) charge separation in the reaction center (k_{CS}), 3) charge recombination — leading to regeneration of excited state in RC from the (dark) charge separated state (k_{CR}), 4) secondary (irreversible) charge separation — leading to formation of stable (dark) radical pair state (k_{RP}). At this point, the nature of the primary and secondary charge separated states does not have to be specified.

The network of light-harvesting complexes (nodes) and links is presented in Fig. 5. To perform simulations for WT grana membranes it was assumed that 100% of PSII–LHCII supercomplexes are $C_2S_2M_2$ particles as outlined earlier and any effect of the presence of "extra" LHCII trimers was neglected. Neglecting the effect of presence of "extra" LHCII trimers is justified by their low amount in WT grana membranes (0.18 trimers per PSII core i.e. as little as about 4% of total number of Chls *a* associated with $C_2S_2M_2$ complexes per PSII core).

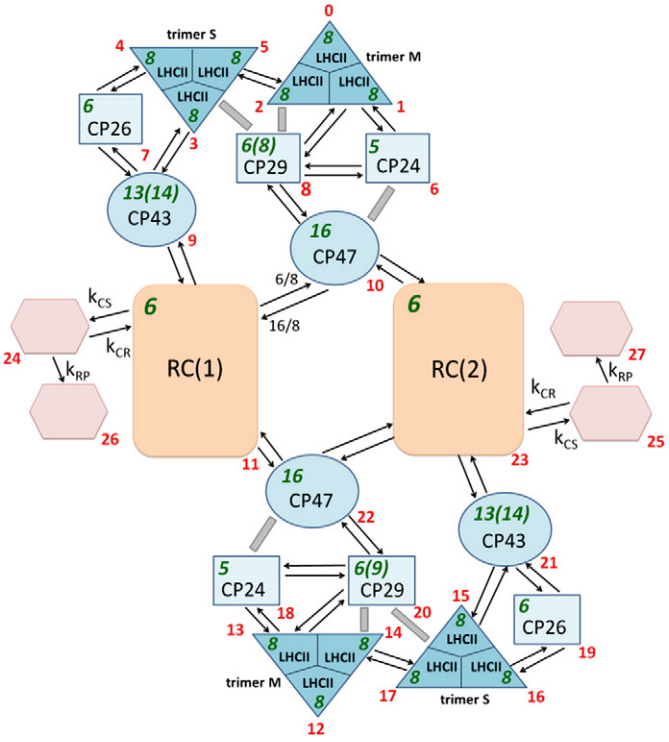

Fig. 5. Network of light-harvesting complexes (nodes 0–23), dark (charge separated) states of RCs (nodes 24–27), and connections between them in the $C_2S_2M_2$ version of the PSII–LHCII supercomplex used in the Monte Carlo simulations of energy and electron transfer processes. The numbers inside the nodes are the numbers of Chls *a*, and the numbers next to each node are the respective nodes' numbers (compare Table 2). When modeling fluorescence decay in the *deg5* mutant, some nodes, together with the corresponding links were removed. Relative values of hopping times between nodes 10 and 11 are shown, as an example, next to the arrows which link these nodes (the values are taken from Table 2). Gray bars represent the extra links, absent from the standard network, and their influence on the lifetime parameters has been tested.

Table 2 presents a full list of light-harvesting complexes (nodes) together with the numbers of Chls *a* in each node and factors to be multiplied by $\tau_{hop} = 1/k_{hop}$ (in last column) in order to calculate actual hopping time from a given light-harvesting complex to all its linked neighbors. Thus, the parameter τ_{hop} represents the intercomplex hopping time between two light-harvesting complexes containing 8 Chls *a* each, for e.g. between two monomers forming any of the LHCII trimers, whereas the actual hopping times between complexes containing different amounts of Chl *a* are modulated by these amounts (Table 2). This approach reflects the situation when excitation transfer from smaller light-harvesting complexes to the larger ones (in terms of number of Chls *a*) is more favorable than in the opposite direction. E.g. the actual hopping time from the small RC node (node 11, only 6 Chls *a*) to its emitting neighbors (nodes 9, 10, 22) is only $(6/8)\tau_{hop}$, whereas the actual hopping time from the large CP47 node (node 10, as many as 16 Chls *a*) to its neighbors is as long as $(16/8)\tau_{hop}$ (see Table 2 and Fig. 5). Such dependence of hopping times on the size of each node (approximated by the numbers of Chls *a* in each node) is equivalent to the assumption that the excitation lifetime in each node is proportional to its size. Such an approach is justified by the previous report demonstrating that all PSII–LHCII subunits are spectrally similar and almost isoenergetic [31]. On the other hand, this approach neglects the presence of minor pool of red-shifted Chls *a* in specific node(s) (see Fig. 4B). Next, we assumed that equilibration between Chls in each node is much faster than excitation hopping between the nodes which was necessary in the coarse-grained model. Most of MC calculations were performed assuming that a single PsbC apoprotein (CP43 complex) binds 13 Chls *a* and Lhcb4 apoprotein (CP29 complex) binds 6 Chls *a*. Therefore the term "standard network" was linked to the network depicted as Fig. 5 with numbers 13 and 6 introduced into nodes representing CP43 and CP29, respectively.

Fig. 6 shows two-exponential fits of fluorescence decay at 688 nm of WT grana membranes measured with streak camera, redrawn from Fig. 4C, together with superimposed curves originating from Monte Carlo (MC) simulations. The detailed description of MC simulations can be found in Appendix B.

The MC-simulated curve obtained for the standard network (see Fig. 5) approximating the WT grana membranes fluorescence decay (bi-exponential) in the best way is presented in Fig. 6 as a thin black line. The four molecular lifetimes underlying this simulated trace, $\tau_{hop} = 10.5$ ps, $\tau_{CS} = 2.0$ ps, $\tau_{CR} = 385$ ps, and $\tau_{RP} = 180$ ps, and related parameters (τ_{mig} and $\Delta G = kT\ln(\tau_{CR}/\tau_{CS})$, see below), are collected in Table 3 (row 1). Parameters τ_{hop} and τ_{CS} may compensate to same extent each other. Therefore, somewhat different combinations of τ_{hop} and τ_{CS}, together with slightly modified two remaining lifetimes, could also give more or less acceptable fits. However, a common feature of all these simulations was relatively deep trap, ΔG, constituted by the primary charge separated state, of ~950 to ~1090 cm^{-1}. Fig. 7 shows the values of τ_{CS} (panel A), τ_{RP}, and ΔG (panel B) yielding the best fits for particular values of τ_{hop}. On panel A, there is additionally shown a normalized sum of squares (sos) parameter being a measure of simulation quality. As can be seen, the highest quality simulations (the lowest sum of squares values) can be obtained for the τ_{hop} values ranging from ~4.5 to ~10.5 ps (Fig. 7A). The corresponding τ_{CS} values range from ~4 to ~2 ps (Fig. 7A). For values being out of this range, the quality of simulations is steeply getting worse. Inset in Fig. 6 allows comparison of the simulations' quality of the two relatively best combinations of parameters ($\tau_{hop} = 4.5$ ps and $\tau_{CS} = 4$ ps vs. $\tau_{hop} = 10.5$ ps and $\tau_{CS} = 2$ ps). It is worth to note that deviations between the fit and the simulated curves are more uniformly distributed in the case of $\tau_{hop} = 10.5$ ps, whereas for $\tau_{hop} = 4.5$ ps the deviations are more systematic. This observation favors the former simulation. Similar sum of squares parameter shown

Table 2
Properties of PSII light-harvesting complexes taken into account in modeling of energy and electron transfer in PSII–LHCII supercomplex.

Node number	Node (light-harvesting complex or dark state)	Number of Chls *a* in the given node	Lifetime parameters: hopping time (in τ_{hop} [ps] units) and electron transfer lifetimes
0	Monomer LHCII M (1)	8	1
1	Monomer LHCII M (1)	8	1
2	Monomer LHCII M (1)	8	1
3	Monomer LHCII S (1)	8	1
4	Monomer LHCII S (1)	8	1
5	Monomer LHCII S (1)	8	1
6	Lhcb 6 (1) CP24	5	5/8
7	Lhcb 5 (1) CP 26	6	6/8
8	Lhcb 4 (1) CP 29	6 (8)	6/8 (1)
9	CP 43 (1)	13 (14)	13/8 (14/8)
10	CP 47 (1)	16	16/8
11	RC(1)	6	6/8, τ_{CS}
12	Monomer LHCII M (2)	8	1
13	Monomer LHCII M (2)	8	1
14	Monomer LHCII M (2)	8	1
15	Monomer LHCII S (2)	8	1
16	Monomer LHCII S (2)	8	1
17	Monomer LHCII S (2)	8	1
18	Lhcb 6 (2) CP24	5	5/8
19	Lhcb 5 (2) CP 26	6	6/8
20	Lhcb 4 (2) CP 29	6 (9)	6/8 (9/8)
21	CP 43 (2)	13 (14)	13/8 (14/8)
22	CP 47 (2)	16	16/8
23	RC(2)	6	6/8, τ_{CS}
24	Dark state 1 — RC(1)	–	τ_{CR}, τ_{RP}
25	Dark state 1 — RC(2)	–	τ_{CR}, τ_{RP}
26	Dark state 2 — RC(1)	–	
27	Dark state 2 — RC(2)	–	

Lifetimes τ_{CS}, τ_{CR}, and τ_{RP} are reciprocals of the respective rate constants shown in Fig. 5 and together with τ_{hop} constitute the parameters being optimized during the fitting procedure.

in Fig. 7A for these two simulations results from the limitations of our MC simulation method: as can be seen in the inset in Fig. 6, the first steps of simulated decay with fast charge separation (2 ps) are of stair-like shape with steep steps caused by discrete lifetimes of excitation energy transfer from reaction center nodes (node numbers 11 and 23 in Fig. 3) to the primary charge separation states nodes (nodes numbers 24 and 25). These initial artificial "stairs" make the simulation quality poorer than it should be. Parameters of the simulation for the "sim 4.5/4/400/130" curve (inset in Fig. 6) are also presented in Table 3 (row number 4). Panel B in Fig. 7 shows systematic but small tendency of both τ_{RP} and ΔG parameters to decrease with decreasing τ_{hop}. It should be underlined that the deep ΔG gap is absolutely necessary in order to obtain good quality of our simulations. Moreover, the deep trap (or long lifetimes of charge recombination relative to primary charge separation) is apparently the most obvious difference between the molecular parameters found previously ([3,6]; row numbers 7 and 8 in Table 3) and in this work (row numbers 1 and 4), explaining the experimentally observed significantly faster fluorescence decay in our case.

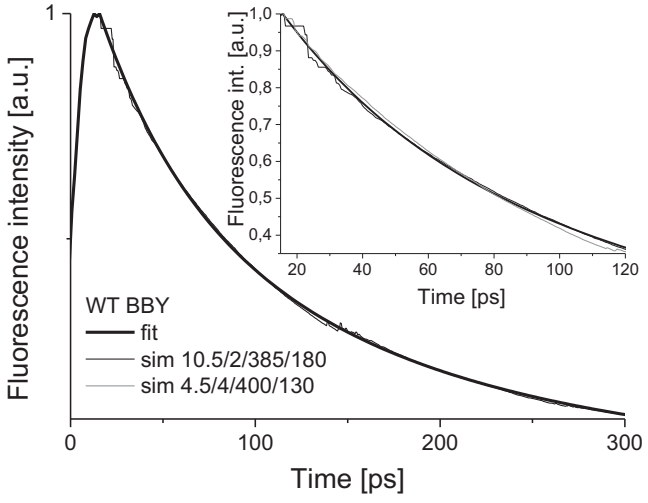

Fig. 6. Experimental fit and Monte Carlo modeled fluorescence decays in WT grana membranes. The parameters of the best quality simulation (denoted "sim 10.5/2/385/180") performed using the standard network (see Fig. 5) are the following: τ_{hop} = 10.5 ps, τ_{CS} = 2.0 ps, τ_{CR} = 385 ps, and τ_{RP} = 180 ps (Table 3, row 1). Inset: first 120 ps of the two-exponential fit to the experimental fluorescence decay of WT grana membranes with superimposed two MC-simulated curves corresponding to the two sets of parameters shown in Table 3 (rows 1 and 4).

The last parameter calculated in MC simulations shown in Fig. 7C, mean migration time (τ_{mig}) from anywhere in the PSII antenna to one of the reaction center nodes, depends linearly on hopping time. For the two limiting sets of the remaining parameters characterized by low sos values, the τ_{mig} equals 32 ps and 72 ps (Table 3). Extending somewhat this range to 30–80 ps and comparing it to the average fluorescence lifetime τ_{av} = ~120 ps (Table 1) one may safely conclude that the excitation migration to the reaction centers takes 25% to 67% of the total excitation lifetime in the antenna system. The remaining time of excitation lifetime ($\tau_{av} - \tau_{mig}$) = 40–90 ps would result from the bottleneck effect of the charge separation in the reaction center.

At this point it is important to note that all the discussed above values of parameters have been obtained for the standard network presented in Fig. 5. In order to go out of the constraints put on by this particular network we tested two other somewhat modified networks.

First, we increased the amounts of Chls a in a few nodes (nodes 8, 9, 20, 21 — see numbers of Chls *a* in brackets in Table 2) in line with a few recent reports (see Table A1 in Appendix A). This leads to increase of the total number of Chls *a* in the $C_2S_2M_2$ form of PSII–LHCII dimeric supercomplex from 200 to 207. As could be expected and as can be seen in Table 3 (row number 2), the only effect of such a modification on MC simulation results is slight acceleration of hopping time from 10.5 to 10 ps.

Secondly we tested introducing to the standard network six extra links between the nodes shown in Fig. 5 as gray bars. Similar extra connections were considered by [3]. One may expect that the extra links makes the overall excitonic coupling stronger and accelerate excitation migration towards the reaction center. This expectation is confirmed by the MC simulations: in order to compensate the accelerated by the extra links excitation flow towards the reaction center, the hopping time was increased from 10.5 to 12.5 ps. Importantly however, the remaining parameters including mean migration time, τ_{mig} were unchanged (Table 3, row number 3) similarly as it was the case when introducing extra Chls *a*.

Finally, we took into account a possibility that excitations in the peripheral antennas may be equilibrated not only over Chls *a* but also over Chls *b* as demonstrated experimentally by [27,29]. Since the site energy of Chl *b* is at room temperature at least 2.5 kT (k — Boltzmann constant, T — temperature) higher than that of Chl *a*, the probability of exciton localization on Chl *b* is at least 10 times lower than on Chl *a*. Taking into account this number and regarding that the number of Chl *b* molecules in PSII–LHCII supercomplex is about 90, one can estimate that 90 Chls *b* are equivalent (in terms of excitation probability) to about 10 extra Chl *a* molecules. Consequently, we performed additional simulations for the standard network increased by 10 Chls *a*, thus increasing the total number of Chls *a* from 200 to 210 (compare Fig. 5). We decided to place the extra single Chls *a* in the nodes (light-harvesting complexes) in which the relative amount of Chls *b* is the highest (nodes 0, 1, 3, 4, 6, 12, 13, 15, 16, 18). An introduction of extra Chls *a* to calculations allowed to obtain a fit which is of similar quality to the one described for the standard network, with the only difference consisting in accelerating hopping time to τ_{hop} = 9 ps. This effect is qualitatively similar to the addition

Table 3
The values of simulation parameters yielding the best fits of model curves to the experimental fluorescence decays at 688 nm in WT and mutant grana membranes. Two of the model curves (rows 1 and 4) are shown in Fig. 6 as superimposed on fits of experimental decays.

	Sample	τ_{hop} [ps]	τ_{CS} [ps]	τ_{CR} [ps]	τ_{RP} [ps]	τ_{CR}/τ_{CS}	ΔG (cm^{-1})	τ_{mi} [ps]	Comments
1	*WT*	**10.5**	**2.0**	**385**	**180**	**192**	**1090**	**72**	Standard network (sn) *A. thaliana*, 298 K
2	*WT*	10.0	2.0	385	180	192	1090	72	sn + 7 extra chlorophylls *A. thaliana*, 298 K
3	*WT*	12.5	2.0	385	180	192	1090	71	sn + 6 extra links *A. thaliana*, 298 K
4	*WT*	4.5	4.0	400	130	100	950	32	sn *A. thaliana*, 298 K
5	*deg5*	5.0	3.5	1000	130	286	1170	32	sn, *A. thaliana*, 298 K 50% *WT* (10.5/2/385/180)
6	*WT* [5]	17	1.24	$143 \cdot 10^3$	13.3	$115 \cdot 10^3$	2380	–	Spinach, 293 K
7	*WT* [6]	3.5	5.5	345	137	63	826	34.5	Spinach, 286 K
8	*WT* [6] refitted in [3]	5.6	4.1	188	113	46	764	–	Spinach, 286 K

Energy gap ΔG between excited state of RC and primary charge separated is related to τ_{CS} and τ_{CR} by the Boltzmann distribution given by the formula: $\Delta G = kT \ln(\tau_{CR}/\tau_{CS})$, where k is the Boltzmann constant and T is the absolute temperature. Standard network (sn) is that one shown in Fig. 5 (without six extra links shown as gray rectangles). 7 extra chlorophylls *a* are located in light-harvesting complexes CP29 and CP43 (see Table 2 and Fig. 5, numbers in brackets in the respective nodes). In bold: parameters of the MC simulation yielding the best quality fit.

of 7 extra Chls *a* to CP29 and CP43, as described above. Thus including the exciton equilibration over all Chls present in the nodes leads to a slight acceleration of hopping, without changes in kinetics of electron transfer.

We conclude that the biexponential shape of the fluorescence decay is largely determined by the electron transfer parameters in the reaction center, especially by ratio of τ_{CR}/τ_{CS} (or ΔG) and also by τ_{RP}, whereas the details of the antenna excitation transfer – exact numbers of Chls a in particular nodes and possible extra links – are of minor significance and only slightly modify hopping time. As discussed above there is still a bit of room in simulations for some compensation between τ_{hop} and τ_{CS}.

3.5. Comparison of Monte Carlo simulations with the results of previous analytical modeling

The parameters resulting from MC simulations described in Subsection 3.4 were compared with those reported previously for spinach grana membranes (Table 3, rows 6–8; [3,5,6]).

The set of lifetime parameters published by [5], presented in Table 3 (row 6) reflects the situation of almost irreversible primary charge separation with a very deep free energy gap of 2380 cm^{-1}. The consequence of this irreversibility was the large τ_{hop} value of 17 ps. On the basis of measurements with selective excitation of Chls *a* or Chls *b*, the same group published improved set of parameters, the main differences being shallower charge separation state trap ($\Delta G = 826$ cm^{-1}), faster hopping ($\tau_{hop} = 3.5$ ps) and slower charge separation ($\tau_{CS} = 5.5$ ps) (Table 3). Later on, these parameters were recalculated yielding $\Delta G = 764$ cm^{-1}, $\tau_{hop} = 5.6$ ps, and $\tau_{CS} = 4.1$ ps ([3], Table 3). Interestingly, despite significantly faster experimental fluorescence decay measured by us ($\tau_{av} \approx 120$ ps vs. $\tau_{av} \approx 150$ ps; Table 1) the sets of parameters obtained from MC simulations by us are not much different from those published by [3]. Especially the set including $\tau_{hop} = 4.5$ ps and $\tau_{CS} = 4.0$ ps (Table 3, row 4) resembles the values reported by [3]. Also calculated migration times are similar for the compared sets: 32 ps in our case vs. 34.5 ps in the paper by [6] (Table 3). Consequently, we regard a deeper trap of $\Delta G = 950$ cm^{-1} to be the main factor responsible for the overall faster decay in our case. This gap is even deeper, $\Delta G = 1090$ cm^{-1}, for better quality MC simulation yielding the parameters shown in Table 3, row 1.

At this point it is worth to refer to older data indicating that PSII is a "shallow trap" (e.g. [32–34]). In fact the "deepness of the PSII trap" depends on how this term is defined. In this paper, the free energy gap that is considered, is the free energy difference between the primary charge separated state and excited state equilibrated over the reaction center. However, in general the gap may be calculated as the difference between the energies of the primary charge separated state and excited state localized on a single pigment or equilibrated over a bigger set of antenna pigments according to the formula:

$$\Delta G = k_B T \ \ln(k'_{CS}/k_{CR}), \tag{1}$$

where k'_{CS} is an apparent charge separation rate constant, k_{CR} is charge recombination rate constant, k is Boltzmann constant, and T is absolute temperature. The apparent rate k'_{CS} depends on the size of the system over which equilibration is assumed to occur and decreases with increasing size of the system. In a limit case of a single absorbing molecule being at the same time the primary electron donor, the rate k'_{CS} adopts the highest value, called intrinsic charge separation rate constant, $k_{CS,int}$ [32]. Considering simplified system of N isoenergetic absorbing (antenna) molecules over which excitation is equilibrated before charge separation takes place, one can write:

$$k'_{CS} = k_{CS,int}/N, \tag{2}$$

meaning that the probability of excitation localization on the primary electron donor molecule equals 1/N. Combining Eqs. (1) and (2) one can write:

$$\Delta G = kT \ \ln\left(k_{CS,int}/k_{CR}\right) - kT \ \ln N, \tag{3}$$

where the term $\Delta G_{int} = kT \ln(k_{CS,int}/k_{CR})$ may be called intrinsic energy gap and is independent of the size of antenna system being in equilibrium with the primary donor, and the entropy term kT lnN increases with N.

It is important to notice that Schatz et al. [32] who studied PSII particles from *Synechococcus* sp. containing 80 Chls *a*, assumed that the whole antenna system was in equilibrium with the primary charge separated state (radical pair equilibrium model). On the other hand, it was assumed by us that the equilibration leading to primary charge separation occurs among only 6 Chls *a* localized in RC. A consequence of the differences in the approaches used is that the entropy term (Eq. (3)) resulting from the work by Schatz et al. [32] is by ~520 cm^{-1} (~65 meV) larger than that one calculated according to our approach, leading to smaller ΔG in the former case. Thus, direct comparison of the shallow PSII RC trap of ~300 cm^{-1} (~38 meV) proposed by Schatz et al. [32] with the deep trap of ~1000 cm^{-1} (~125 meV) which is reported in our paper would be improper. In order to correct the Schatz et al. data [32] and make them comparable with our results one could propose to extrapolate their calculations to the antenna system diminished to 6 Chls a. Such a correction would yield the energy gap of (300 cm^{-1} + 520 cm^{-1}) = 820 cm^{-1}, which is very similar to the values reported by Broess et al. [6] and Caffarri et al. [3] and not very much different from 1000 cm^{-1} reported in this paper. The remaining

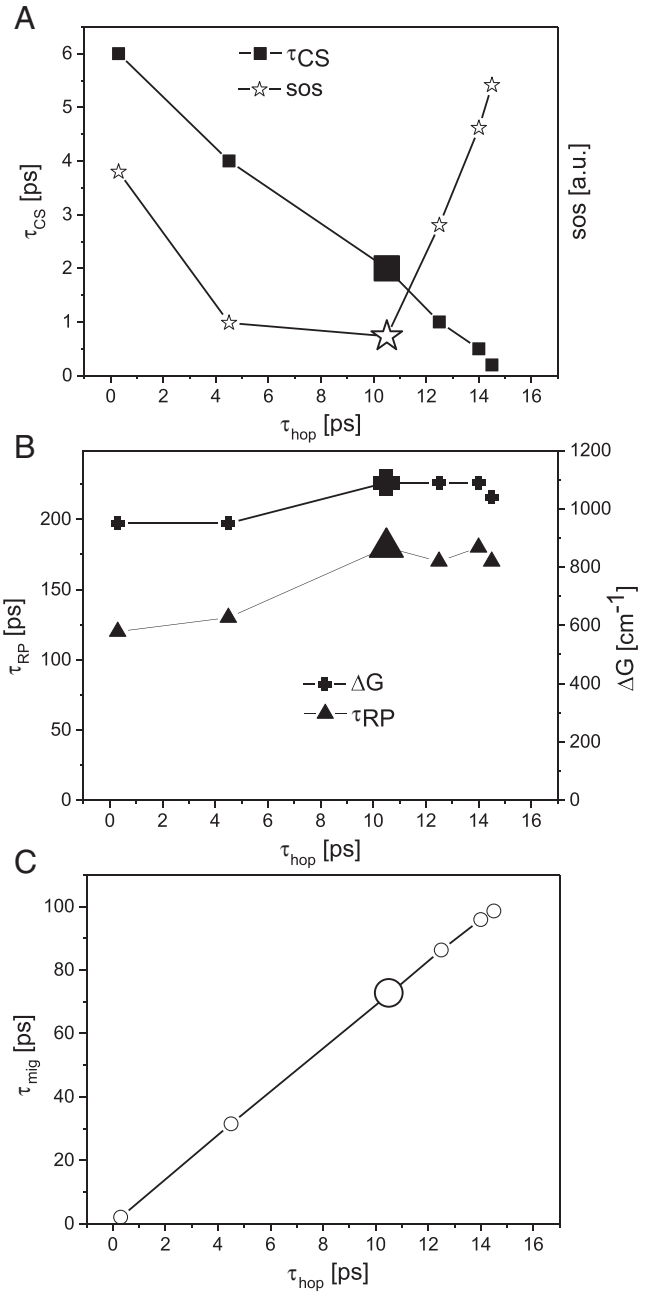

Fig. 7. Lifetime and energetic parameters yielding the best fits of Monte Carlo curves to the experimental fluorescence decay of WT grana membranes at 688 nm measured with the streak camera for a range of τ_{hop} values. (A) Apart from the dependence of τ_{CS} on τ_{hop}, there is a plotted normalized sum of squares (sos) parameter calculated as $\Sigma(f(x_i) - s(x_i))^2$ / N, where $f(x_i)$ is the two-exponential fit to the experimental fluorescence decay of WT BBY at 688 nm following excitation at 400 nm (see Table 1), $s(x_i)$ is the MC-simulated decay on the basis of the lifetime parameters shown in panels A and B, and N is the number of points contributing to the sum (i = 1.. N). (B) Apart from the dependence of τ_{RP} on τ_{hop}, there is a shown dependence of ΔG on τ_{hop}. τ_{mig} and ΔG are calculated from the lifetime parameters. (C) Mean migration time to the RC nodes (τ_{mig}) as a function of τ_{hop}. The big symbols in all panels represent a set of parameters giving the best fit: τ_{hop} = 10.5 ps, τ_{CS} = 2 ps, τ_{CR} = 385 ps, τ_{RP} = 180 ps.

difference of ~200 cm^{-1} could be a consequence of different raw experimental results underlying the two studies.

In more recent studies performed on PSII core complexes isolated from *Thermosynechoccocus elongatus* it was proposed that the first charge separated state was $Chlacc_{D1}^{+}Pheo_{D1}^{-}$, quickly followed by the second charge separated state, $P_{D1}^{+}Pheo_{D1}^{-}$, and then followed by the state $P_{D1}^{+}Q_A^{-}$, all the states being in equilibrium [35–37]. P_{D1} is one of the chlorophyll dimer components, $Pheo_{D1}$ is pheophytin, and $Chlacc_{D1}$ is a monomeric chlorophyll placed in between P_{D1} and $Pheo_{D1}$, all the molecules being associated with D_1 polypeptide of RC. The free energy gap between excited state of reaction center, RC*, and the state $P_{D1}^{+}Pheo_{D1}^{-}$ calculated in the cited papers was about 880 cm^{-1} (110 meV) which is again similar to the value of 1000 cm^{-1} estimated by us. It is understandable that the free energy gap between the states RC* and $Chlacc_{D1}^{+}Pheo_{D1}^{-}$ was found to be smaller and equal ~320 cm^{-1} [35–37]. However, in our studies we have not been able to resolve the additional relatively short lived (~10 ps according to [35]), $Chlacc_{D1}^{+}Pheo_{D1}^{-}$ intermediate state. We conclude that the trapping properties of RC reported in this paper are not very much different from those reported previously by others.

3.6. Fluorescence decay in deg5 mutant grana membranes

Both streak camera and TC-SPC measurements show clearly that the removal of ~25% of Lhcb6 apoprotein pool (CP24) from PSII–LHCII supercomplexes in grana membranes of *deg5* mutant of *A. thaliana* leads to a significant acceleration of fluorescence decay with respect to WT grana membranes (Fig. 8A–C); relevant fluorescence decay kinetics for WT and *deg5* grana membranes are shown as Fig. 8D–F and parameters of the fits, lifetimes and relative amplitudes are displayed in Table 4. A juxtaposition of the data included in Table 1 (WT) and Table 4 (*deg5*) reveals that as a rule, partial Lhcb6 apoprotein removal is accompanied by a remarkable decrease in average fluorescence lifetimes, no matter whether streak camera or TC-SPC approaches was applied (e.g. from 120 to 102 ps when using streak camera with the fluorescence detection at 688 nm). The accelerated fluorescence decay in the mutant deficient in Lhcb6 apoprotein is due both to shortening of the slower decay component and its lower relative amplitude (Fig. 8A and B). Importantly, the shapes of the both DAS, fast 47/52 ps and slow 165/149 ps, are very similar in *deg5* mutant and WT plant (Fig. 8C) and this supports the notion that the mutation does not lead to major general changes in spectroscopic features. Interestingly, the stronger mutation, leading to 100% removal of Lhcb6 apoprotein pool in *A. thaliana* caused a deceleration of fluorescence decay [4]. The difference between the data may be due to different mutation-related rearrangements in PSII–LHCII supercomplex antenna system and "extra" LHCII pool.

3.7. Monte Carlo simulations for deg5 grana membranes

3.7.1. Simulation of the effect of removal of CP24 and LHCII-M trimers on fluorescence decay kinetics

In order to stimulate fluorescence decay kinetics found for *deg5* grana membranes we removed CP24 and LHCII M trimer, either from one or both sides of the PSII–LHCII supercomplex (Fig. 5) keeping unchanged all the lifetime parameters determined for WT grana membranes (Table 3, row 1 or row 4 or similar). As a result, the modeled kinetics was found to be comparable or even faster than the one measured for the mutant. However, in order to take into account that the mutant is lacking as little as ~25% of Lhcb6 apoprotein pool, the decays approximating the experimental kinetics in *deg5* mutant were calculated (see Subsection 3.1): (1) either as a weighted average of decay simulated for the standard network missing one CP24 complex and one nearby LHCII-M trimer (weight 50%) and the decay found for WT (weight 50%) — see Fig. 9; (2) or as a weighted average of decay simulated for the standard network missing both CP24 complexes and both LHCII-M trimers (weight 25%) and the decay found for WT (weight 75%). The two modeled kinetics were similar to each other whereas the simulated mean decays, although significantly accelerated with respect to WT grana membranes, were still slower than the kinetics measured for *deg5* grana membranes (Fig. 9).

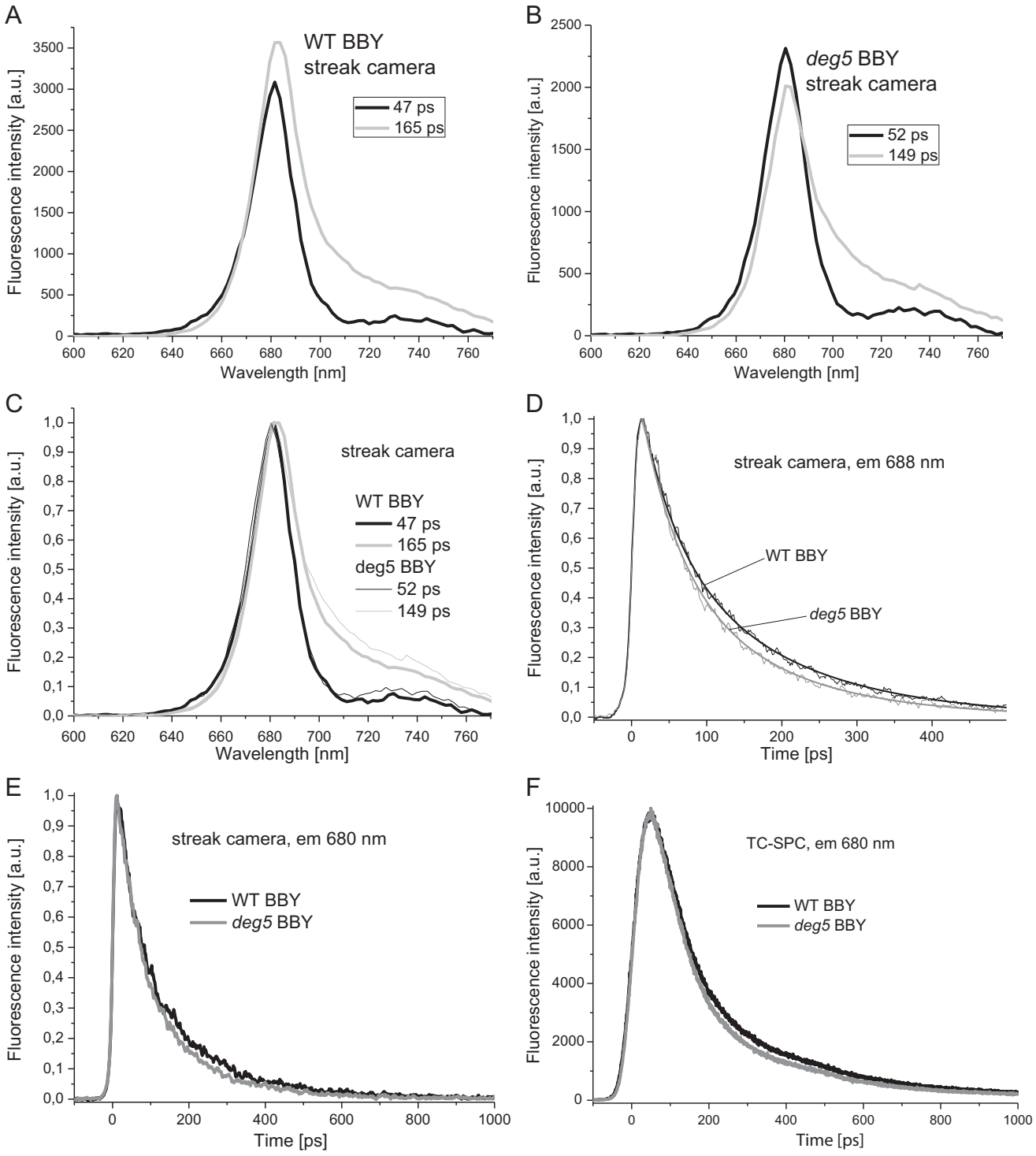

Fig. 8. Comparison of fluorescence decay associated spectra and fluorescence decay kinetics for WT and *deg5* mutant grana membranes. (A, B) — fluorescence decay associated spectra for WT and *deg5*; (C) — fluorescence decay associated spectra for WT and *deg5* as normalized to the same amplitude at maximum; (D–F) fluorescence decay kinetics for WT and *deg5* detected at 688 (streak camera) or 680 nm (streak camera or TC-SPC approach). Excitation wavelength was set at 400 nm.

For the case when 50% of the mutant PSII–LHCII supercomplexes are represented by C_2S_2M form (lacking a single CP24 copy and a single LHCII-M trimer) a fluorescence decay kinetics for *deg5* grana membranes was alternatively modeled assuming that lifetime parameters of partially truncated PSII–LHCII supercomplexes (C_2S_2M) may be changed with respect to $C_2S_2M_2$ form of supercomplexes (constituting remaining 50% of the mutant supercomplexes pool), which have the parameters equal to the ones calculated for WT grana membranes. The simulation that fits the experimental decay in the best way was obtained using the following lifetime parameters for the truncated supercomplexes: $\tau_{hop} = 5.0$ ps, $\tau_{CS} = 3.5$ ps, $\tau_{CR} = 1000$ ps, and $\tau_{RP} = 130$ ps (see Table 3, row 5). It is interesting to note that this set of parameters is similar to one of the sets found for the WT grana membranes (Table 3, row 4). The main difference is significantly higher value of $\tau_{CR} = 1000$ ps, suggesting that the reaction center trap in the truncated supercomplexes is significantly deeper ($\Delta G = 1170$ cm^{-1}) than in the $C_2S_2M_2$ supercomplexes.

Table 4
Comparison of parameters of fluorescence decay kinetics detected at 688 and 680 nm obtained for *deg5* mutant BBY membranes using two experimental approaches.

λ_{em} [nm]	Technique	IRF [ps]	FWHM [ps]	τ_1 [ps] (A_1)	τ_2 [ps] (A_2)	τ_3 [ps] (A_3)	τ_{av} [ps]
688	**Streak**	**3**	**75**	**52 (0.48)**	**149 (0.52)**	**–**	**102** ($n = 2$; 102–103)
680	Streak	3	75	52 (0.54)	149 (0.46)	–	97 ($n = 2$; 97)
	TC-SPC	42	146	47 (0.573)	138 (0.400)	625 (0.027)	99 ($n = 4$; 92–111)

The parameters were determined the same way as those shown in Table 1. In bold: parameters of the fluorescence decay curve simulated in the MC method.

3.7.2. Simulation of the effect of removal of CP24 and LHCII M trimers on fluorescence decay kinetics with the assumption that energy connection between CP24/LHCII-M and the remaining part of the supercomplexes is weak

Alternatively, we assumed that both CP24/LHCII-M complexes present per dimeric PSII–LHCII supercomplex are weakly coupled to the remaining part of the supercomplex i.e. that the energy transfer between CP24–LHCII-M complex and the remaining part is slow in $C_2S_2M_2$ supercomplexes. As a consequence, hopping between the remaining light-harvesting complexes (i.e. other than CP24 and LHCII-M trimer) would have to be faster to fit the experimental decay in WT grana membranes. Therefore, removal of weakly connected CP24–LHCII-M complexes in part of PSII–LHCII supercomplexes should cause a significant acceleration of the decay modeled for *deg5* grana membranes. Indeed, such an effect has been observed: the slower was the energy transfer between CP24/LHCII-M trimer complex and the remaining part of the supercomplex, the faster was hopping time between the remaining complexes in WT grana membranes. In order to get good fits, it was necessary, however, to reoptimize parameters other than hopping time, as well. For example, a constraint of 30-times deceleration of energy transfer between CP24/LHCII-M complex and the remaining part of the supercomplexes resulted in the following set of parameters: $\tau_{hop} = 3.9$ ps, $\tau_{CS} = 4.0$ ps, $\tau_{CR} = 1000$ ps, and $\tau_{RP} = 130$ ps, fitting relatively well the experimental decay in WT grana membranes. However, even such a strong slowing down of hopping between CP24–LHCII-M and the remaining part of the supercomplex was not enough to exactly fit the experimental decay in the mutant grana membranes, i.e. after removal of 25% of (weakly bound) CP24–LHCII-M from $C_2M_2S_2$ in the MC simulation, the resulting decay, although accelerated compared to the WT grana membranes, was slower than the experimental fluorescence decay in the mutant grana membranes.

Thus performing the alternative simulations described in Subsections 3.7.1 and 3.7.2 allows concluding that speeding up of fluorescence decay in *deg5* mutant grana membranes with respect to that of WT may be caused by a combination of two effects: decreased antenna system and a deeper trap constituted by the primary charge separated state in a fraction of partially truncated PSII–LHCII supercomplexes.

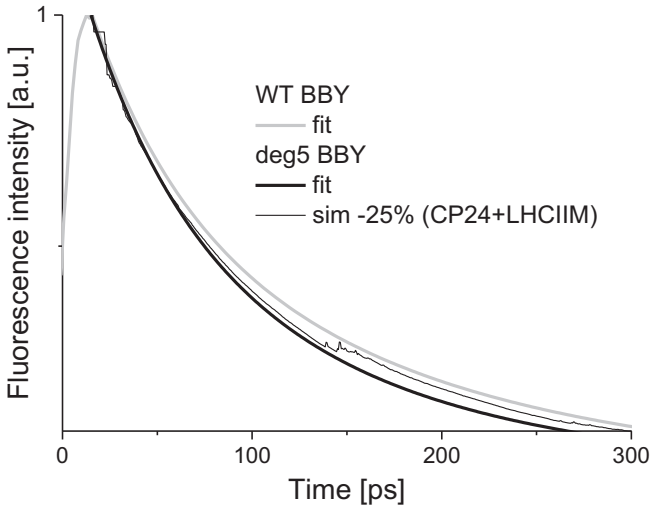

Fig. 9. Experimental fits to fluorescence decays in WT and *deg5* grana membranes and Monte Carlo-modeled curve for *deg5* grana membranes. The simulated curve (denoted "sim −25% (CP24 + LHCIIM")) was calculated as the arithmetic mean of (1) decay simulated for WT (with parameters from Table 3, row 1) and (2) decay simulated for the standard network missing CP24 and LHCII-M complexes (nodes 0, 1, 2, and 6) with the same lifetime parameters as those used for WT simulation.

3.7.3. Contribution from "extra" LHCII trimers

According to MC simulation described above, *deg5* grana membranes contain more "extra" LHCII trimers (i.e. trimers not coupled to the supercomplex) per PSII core dimer (0.78) than those of WT grana (0.36), although a total number of LHCII trimers per PSII core dimer (i.e. including those associated as S trimers and M trimers with PSII–LHCII supercomplexes and the "extra" ones) is almost identical for the two genotypes (4.28 vs. 4.36, respectively), as outlined in Subsection 3.1. Since the "extra" LHCII trimers were not a subject of MC simulations, it cannot be a priori excluded that fast excitation quenching in the this pool of LHCII trimers contributes to the accelerated fluorescence decay in the *deg5* grana membranes. At first glance it seems to contradict the suggestion that grana regions enriched in "extra" LHCII trimers detected in koCP24 mutant [25] have considerably slower fluorescence decay with regard to $C_2S_2M_2$ complexes [4]. The reason for this discrepancy may be related to the difference in aggregation state of "extra" LHCII trimers in koCP24 mutant and *deg5* one. In vitro, aggregation of purified LHCII trimers was shown to render fluorescence decay considerably faster with respect to unaggregated trimers [30] thus "extra" LHCII trimers detected in koCP24 mutants may be regarded as largely unaggregated whereas "extra" LHCII trimers present in grana membranes of *deg5* mutant as (partially?) aggregated ones.

It is highly probable that "extra" LHCII trimers of the two mutants differ considerably with respect to their polypeptide composition. Namely, the results presented in Subsection 3.1 of this work strongly suggest that these are typical LHCII-M trimers that build up "extra" LHCII pool of *deg5* mutant while the "extra" trimers present in grana membranes of koCP24 mutant may be atypical, since Lhcb3 apoproteins of the mutant's LHCII-M trimers seem to be at least partially substituted by Lhcb1 and Lhcb2 ones as judged by a decrease in Lhcb3 and a compensatory increase in Lhcb1/Lhcb2 pools demonstrated to occur simultaneously in the koCP24 mutants vs. WT plants [25,26]. Since individual LHCII apoproteins are heterogeneous with regard to the rate of cation-induced aggregation in vitro [38] typical and atypical "extra" LHCII-M trimers may be represented by quite different aggregation states in vivo and have opposite impacts on fluorescence decay of grana membranes.

Acknowledgements

This work was supported by the Polish National Science Center through grant no. N N303 563539 to GJ. WG, SS, EG, and WS were supported by Laserlab-Europe, the Integrated Initiative of European Laser Research Infrastructures in the 7-th Framework Programme of EU (grant nos. LCVU001717 (2011) and LLAMS001882 (2012)). KG was supported by the project "Integrated program supporting the development of the Adam Mickiewicz University in Poznan in the field of physical sciences: Pro-innovative education, competent staff, graduates of the future" (POKL.04.01.01-00-133/09-00 Sub-measure 4.1.1 of the Human Capital Operational Programme, co-financed by the European Union under the European Social Fund).

Appendix A. Calculation of PSI/PSII ratio for grana membranes

To calculate *PSI*/*PSII* ratio, the Chl *a*/apoprotein and Chl *b*/apoprotein stoichiometry of the individual pigment–protein complexes belonging to PSII–LHCII supercomplexes ($C_2S_2M_2$) [39–42] and PSI–LHCI supercomplexes [43,44] (see Table A1) as well as Chl *a*:Chl *b* ratio and the number of LHCII trimers per PSII core (n) determined experimentally for wild type and *deg5* grana membranes in this work, were applied.

Table A1
Literature numbers of Chl *a* and Chl *b* molecules in PSII polypeptides and PSI–LHCI complex.

Pigment–protein complex	Number of Chl *a* molecules associated with the complex per P680 or P700	Number of Chl *b* molecules associated with the complex per P680 or P700	Source
PSII reaction center	6		[40,44]
CP47	16	–	
CP43	13 or 14		
CP24	5	4	[38]
CP26	6	3	
CP29	6 or 8.5	2 or 4.5	[38,41]
LHCII trimer	24	18	[39]
PSI–LHCI	155.7	17.3	[42,43]

For instance, when the number of Chl *a* molecules associated with CP43 per P680 equals 13 [41] and the number of Chl *a* and Chl *b* molecules associated with CP29 per P680 equals 8.5 and 4.5, respectively [42], the Chl *a*:Chl *b* ratio (A), for both wild type and *deg5* grana membranes is given by a following equation:

$$A = \frac{155.7PSI + 35PSII + 19.5PSII + 24nPSII}{17.3PSI + 11.5PSII + 18nPSII}. \quad (A1)$$

In turn, when the number of Chl *a* molecules associated with CP43 per P680 is taken as 14 [45] and the number of Chl *a* and Chl *b* molecules associated with CP29 per P680 again as 8.5 and 4.5, respectively [42], the Chl *a*:Chl *b* ratio (A), for both wild type and *deg5* grana membranes is given by the equation:

$$A = \frac{155.7PSI + 36PSII + 19.5PSII + 24nPSII}{17.3PSI + 11.5PSII + 18nPSII}. \quad (A2)$$

In both equations n represents the number of LHCII trimers per PSII core, PSI is the content value of PSI–LHCI complexes in grana membranes sample and PSII is the content value of PSII–LHCII supercomplexes ($C_2S_2M_2$) in grana membranes sample.

Thus A is given by

$$A = \frac{155.7\frac{PSI}{PSII} + 19.5 + 35 + 24n}{17.3\frac{PSI}{PSII} + 18n + 11.5} \quad (A3)$$

or

$$A = \frac{155.7\frac{PSI}{PSII} + 19.5 + 36 + 24n}{17.3\frac{PSI}{PSII} + 18n + 11.5}, \quad (A4)$$

respectively.

By relevant transformations it is derived that *PSI*/*PSII* can be calculated as

$$\frac{PSI}{PSII} = \frac{24n + 54.5 - A(18n + 11.5)}{17.3A - 155.7} \quad (A5)$$

or

$$\frac{PSI}{PSII} = \frac{24n + 55.5 - A(18n + 11.5)}{17.3A - 155.7}. \quad (A6)$$

Appendix B. Description of Monte Carlo simulation

The network of nodes and links between them considered in MC simulations of fluorescence decay is presented in Fig. 5. Similar nodes and links were used previously [3]. 24 nodes (labeled 0–23 in Fig. 5) correspond to 24 light-harvesting complexes forming the $C_2S_2M_2$ version of the PSII–LHCII supercomplex. They are called emitting nodes, since all of them contain Chl *a* molecules, and their emission may contribute to the fluorescence recorded in the time-resolved experiment. The remaining four nodes (labeled 24–27) correspond to specific charge-separated states of reaction centers, nodes 24 and 25 being primary charge separated states and nodes 26 and 27 being secondary charge separated states. Thus, the nodes 24–27 depict non-emitting or dark states of RCs. Back transitions from nodes 24 and 25 to the emitting nodes (nodes 11 and 23 representing excited states of RCs) are possible, whereas transitions to nodes 26 and 27 are irreversible.

In order to simulate fluorescence decay in the $C_2S_2M_2$ version of the PSII–LHCII supercomplex the following algorithm was applied. It was assumed that the initial single photon excitation of any of the emitting nodes randomly walks between nodes until it reaches one of the final dark state (nodes 26 or 27). The initial excitation was randomly placed in one of the emitting nodes (0–23) with the probability of n/N, where n is the number of Chls *a* in the given node and N is the number of all Chls a in the $C_2S_2M_2$ version of the PSII–LHCII supercomplex (N = 200 for the standard network). This approach is justified by the fact that excitation flashes, at 400 nm, are not expected to excite significant amount of Chls *b*. The excitation could leave a particular node stochastically with equal probabilities (except for nodes 11, 23–27, see below) to one of the neighboring linked node after time interval specified in Table 2 divided by the number of linked neighbors.

After reaching one of the RC nodes (11 and 23), excitation could be quenched with rate $k_{cs} = 1/\tau_{CS}$ by dark nodes (24 or 25) or be transferred back to any of the three remaining linked nodes with equal rates $1/0.75 * \tau_{hop}$ (see Table 2). Effectively, the excitation was transferred from nodes 11 and 23 to one of the neighboring nodes after time resulting from summation of the rates and given by the formula:

$$\tau_{11,23} = \frac{1}{\frac{1}{\tau_{CS}} + \frac{3}{0.75 * \tau_{hop}}}. \quad (B1)$$

Consequently, probabilities of charge separation, P_{CS}, and of excitation escape via each of the three remaining pathways from RC nodes (11 and 23), P, were calculated, from the following formulas:

$$P_{CS} = \tau_{11,23}/\tau_{CS}, \tag{B2}$$

$$P = \tau_{11,23}/\left(0.75 * \tau_{hop}\right). \tag{B3}$$

Similarly, the lifetime of occupation of dark nodes 24 and 25 was calculated from the formula:

$$\tau_{24,25} = \frac{1}{\frac{1}{\tau_{CR}} + \frac{1}{\tau_{RP}}}, \tag{B4}$$

where τ_{CR} and τ_{RP} are reciprocals of the respective rate constants shown in Fig. 5. The probabilities of charge recombination, P_{CR}, and formation of irreversible radical pair states, P_{RP}, (nodes 26 and 27) were calculated from the formulas:

$$P_{CR} = (1/\tau_{CR})/[(1/\tau_{RP}) + (1/\tau_{CR})], \tag{B5}$$

$$P_{RP} = (1/\tau_{RP})/[(1/\tau_{RP}) + (1/\tau_{CR})]. \tag{B6}$$

The state of the excitation was checked every 0.5 ps from time zero until reaching the final node (26 or 27) and this state was recorded as a function of time: value 1 was assigned to those 0.5-ps time intervals for which excitation was localized on any of the emitting nodes and value 0 — to those intervals for which excitation was localized in the reversible dark state nodes (24 or 25). Recording of the state of excitation in time was repeated about 20 000 times (starting randomly from different emitting nodes), and the sum of all these records, after proper normalization (multiplying by a constant), was compared to the experimentally measured fluorescence decay. Of course, the quality of the simulated fit depended on the values of the four fit parameters τ_{hop}, τ_{CS}, τ_{CR}, and τ_{RP}. After each simulation these parameters were iteratively optimized in order to give possibly best fit of the model curve to the experimental trace.

Appendix C. Supplementary data

Supplementary data to this article can be found online at http://dx.doi.org/10.1016/j.bbabio.2014.12.004.

References

[1] S. Caffarri, R. Kouřil, S. Kereïche, E.J. Boekema, R. Croce, Functional architecture of higher plant Photosystem II supercomplexes, EMBO J. 28 (2009) 3052–3063.
[2] R. Croce, H. van Amerongen, Light-harvesting and structural organization of Photosystem II: from individual complexes to thylakoid membrane, J. Photochem. Photobiol. B Biol. 104 (2011) 142–153.
[3] S. Caffarri, K. Broess, R. Croce, H. Van Amerongen, Excitation energy transfer and trapping in higher plant Photosystem II complexes with different antenna sizes, Biophys. J. 100 (2011) 2094–2103.
[4] B. van Oort, M. Alberts, S. De Bianchi, L. Dall'Osto, R. Bassi, G. Trinkunas, R. Croce, H. van Amerongen, Effect of antenna-depletion in Photosystem II on excitation energy transfer in *Arabidopsis thaliana*, Biophys. J. 98 (2010) 922–931.
[5] K. Broess, G. Trinkunas, C.D. van Der Weij-De Wit, J.P. Dekker, A. van Hoek, H. van Amerongen, Excitation energy transfer and charge separation in Photosystem II membranes revisited, Biophys. J. 91 (2006) 3776–3786.
[6] K. Broess, G. Trinkunas, A. van Hoek, R. Croce, H. van Amerongen, Determination of the excitation migration time in Photosystem II. Consequences for the membrane organization and charge separation parameters, Biochim. Biophys. Acta Bioenerg. 1777 (2008) 404–409.
[7] F.J.E. van Mieghem, G.F.W. Searle, A.W. Rutherford, T.J. Schaafsma, The influence of the double reduction of QA on the fluorescence decay kinetics of Photosystem II, Biochim. Biophys. Acta 1100 (1992) 198–206.
[8] M.J. Schilstra, J. Nield, W. Dörner, B. Hankamer, M. Carradus, L.M.C. Barter, J. Barber, D.R. Klug, Similarity between electron donor side reactions in the solubilized Photosystem II–LHC II supercomplex and Photosystem-II-containing membranes, Photosynth. Res. 60 (1999) 191–198.
[9] R. Kouřil, E. Wientjes, J.B. Bultema, R. Croce, E.J. Boekema, High-light vs. low-light: effect of light acclimation on Photosystem II composition and organization in *Arabidopsis thaliana*, Biochim. Biophys. Acta Bioenerg. 1827 (2013) 411–419.
[10] M. Grabsztunowicz, G. Jackowski, Isolation of intact and pure chloroplasts form leaves of *Arabidopsis thaliana* plants acclimated to low irradiance for studies on Rubisco regulation, Acta Soc. Bot. Polon. 82 (2013) 91–95.
[11] R. Luciński, L. Misztal, S. Samardakiewicz, G. Jackowski, Involvement of Deg5 protease in wounding-related disposal of PsbF apoprotein, Plant Physiol. Biochem. 49 (2011) 311–320.
[12] D.A. Berthold, G.T. Babcock, C.F. Yocum, A highly resolved, oxygen-evolving Photosystem II preparation form spinach thylakoid membranes, FEBS Lett. 134 (1981) 231–234.
[13] T. Dunahay, L.A. Staehelin, M. Seibert, P.D. Ogilvie, S.P. Berg, Structural, biochemical and biophysical characterization of four oxygen evolving Photosystem II preparations from spinach, Biochim. Biophys. Acta 764 (1984) 179–193.
[14] H. Schagger, Tricine-SDS-PAGE, Nat. Protoc. 1 (2006) 16–22.
[15] S.W. Hogewoning, E. Wientjes, P. Douwstra, G. Trouwborst, W. van Ieperen, R. Croce, J. Harbinson, Photosynthetic quantum yield dynamics: from photosystems to leaves, Plant Cell 24 (2012) 1921–1935.
[16] D. Arnon, Copper enzymes in isolated chloroplasts. Polyphenol oxidase in *Beta vulgaris*, Plant Physiol. 24 (1949) 1–15.
[17] W. Giera, V.M. Ramesh, A.N. Webber, I. van Stokkum, R. van Grondelle, K. Gibasiewicz, Effect of the P700 pre-oxidation and point mutations near A_0 on the reversibility of the primary charge separation in Photosystem I from *Chlamydomonas reinhardtii*, Biochim. Biophys. Acta Bioenerg. 1797 (2010) 106–112.
[18] J.J. Snellenburg, S. Laptenok, R. Seger, K.M. Mullen, I.H.M. van Stokkum, Glotaran: a Java-based graphical user interface for the R package TIMP, J. Stat. Softw. 49 (2012) 1–22.
[19] A.R. Holzwarth, Data analysis of time-resolved measurements, in: J. Amesz, A.J. Hoff (Eds.), Biophysical Techniques in Photosynthesis (Advances in Photosynthesis and Respiration), vol. 3, Kluwer Academic Publishers, Dordrecht, 1996, pp. 75–92.
[20] J. Karolczak, D. Komar, J. Kubicki, M. Szymański, T. Wróżowa, A. Maciejewski, Fluorescence dynamics spectrometer of single-picosecond resolution: optimisation of experimental performance, Bull. Pol. Acad. Sci. Chem. 47 (1999) 361–380.
[21] J. Karolczak, D. Komar, J. Kubicki, T. Wróżowa, K. Dobek, B. Ciesielska, A. Maciejewski, The measurements of picosecond fluorescence lifetimes with high accuracy and subpicosecond precision, Chem. Phys. Lett. 344 (2001) 154–164.
[22] T. Wróżowa, B. Ciesielska, D. Komar, J. Karolczak, A. Maciejewski, J. Kubicki, Measurements of picosecond lifetime by time correlated single photon counting method: the effect of the refraction index of the solvent on the instrument response function, Rev. Sci. Instrum. 75 (2004) 3107–3121.
[23] M. Zuker, A.G. Szabo, L. Bramall, D.T. Krajcarski, Delta function convolution method (DFCM) for fluorescence decay experiments, Rev. Sci. Instrum. 56 (1985) 14–22.
[24] X.W. Sun, L. Peng, J. Guo, W. Chi, J. Ma, C. Lu, L. Zhang, Formation of DEG5 and DEG8 and their involvement in the degradation of photodamaged Photosystem II reaction center D1 protein in *Arabidopsis*, Plant Cell 19 (2007) 1347–1361.
[25] S. de Bianchi, L. Dall'Osto, G. Tognon, T. Morosinotto, R. Bassi, Minor antenna proteins CP24 and CP26 affect the interactions between Photosystem II subunits and the electron transport rate in grana membranes of *Arabidopsis*, Plant Cell 20 (2008) 1012–1028.
[26] L. Kovacs, J. Damkjaer, S. Kereiche, C. Illoaia, A.V. Ruban, E.J. Boekema, S. Jansson, P. Horton, Lack of the light-harvesting complex CP24 affects the structure and function of the grana membranes of higher plant chloroplasts, Plant Cell 18 (2006) 3106–3120.
[27] H. Dau, K. Sauer, Exciton equilibration and Photosystem II exciton dynamics — a fluorescence study on Photosystem II membrane particles of spinach, Biochim. Biophys. Acta 1273 (1996) 175–190.
[28] R.C. Jennings, G. Zucchelli, F.M. Garlaschi, The influence of quenching by open reaction centres on the Photosystem II fluorescence emission spectrum, Biochim. Biophys. Acta 1060 (1991) 245–250.
[29] R.C. Jennings_, G. Elli, F.M. Garlaschi, S. Santabarbara, G. Zucchelli, Selective quenching of the fluorescence of core chlorophyll–protein complexes by photochemistry indicates that Photosystem II is partly diffusion limited, Photosynth. Res. 66 (2000) 225–233.
[30] B. van Oort, A. van Hoek, A.V. Ruban, H. van Amerongen, Aggregation of Light-Harvesting Complex II leads to formation of efficient excitation energy traps in monomeric and trimeric complexes, FEBS Lett. 581 (2007) 3528–3532.
[31] R.C. Jennings, R. Bassi, F.M. Garlaschi, P. Dainese, G. Zucchelli, Distribution of the chlorophyll spectral forms in the chlorophyll–protein complexes of Photosystem II antenna, Biochemistry 32 (1993) 3203–3210.
[32] G.H. Schatz, H. Brock, A.R. Holzwarth, Kinetic and energetic model for the primary processes in Photosystem II, Biophys. J. 54 (1988) 397–405.
[33] J.R. Durrant, D.R. Klug, S.L. Kwa, R. van Grondelle, G. Porter, J.P. Dekker, A multimer model for P680, the primary electron donor of Photosystem II, Proc. Natl. Acad. Sci. U. S. A. 92 (1995) 4798–4802.
[34] K. Gibasiewicz, A. Dobek, J. Breton, W. Leibl, Modulation of primary radical pair kinetics and energetics in PS II by the redox state of the quinone electron acceptor Q_A, Biophys. J. 80 (2001) 1617–1630.
[35] A.R. Holzwarth, M.G. Müller, M. Reus, M. Nowaczyk, J. Sander, M. Rögner, Kinetics and mechanism of electron transfer in intact Photosystem II and in the isolated reaction center: pheophytin is the primary electron acceptor, Proc. Natl. Acad. Sci. U. S. A. 103 (2006) 6895–6900.
[36] Y. Miloslavina, M. Szczepaniak, M.G. Müller, J. Sander, M. Nowaczyk, M. Rögner, A.R. Holzwarth, Charge separation kinetics in intact Photosystem II core particles is trap-limited. A picosecond fluorescence study, Biochemistry 45 (2006) 2436–2442.

[37] M. Szczepaniak, J. Sander, M. Nowaczyk, M.G. Müller, M. Rogner, A.R. Holzwarth, Charge separation, stabilization, and protein relaxation in Photosystem II core particles with closed reaction center, Biophys. J. 96 (2009) 621–631.
[38] G. Jackowski, E. Kluck, Heterogeneous behaviour of subunits of the light-harvesting chlorophyll a/b-protein complex of photosystem 2 during cation-induced aggregation, Photosynthetica 29 (1993) 401–407.
[39] R. Bassi, B. Pineau, P. Dainese, J. Marquardt, Carotenoid-binding proteins of Photosystem II, Eur. J. Biochem. 212 (1993) 297–303.
[40] Z. Liu, H. Yan, K. Wang, T. Kuang, J. Zhang, L. Giu, W. Chang, Crystal structure of spinach major light-harvesting complex of Photosystem II at 2.72 Å resolution, Nature 428 (2004) 287–292.
[41] B. Loll, J. Kern, W. Saeneger, A. Zouni, J. Biesiadka, Toward complete cofactor arrangement in the 3 Å resolution structure of Photosystem II, Nature 438 (2005) 1040–1044.
[42] X. Pan, M. Li, T. Wan, L. Wang, C. Jia, Z. Hou, X. Zhao, J. Zhang, W. Chang, Structural insight into energy regulation of light-harvesting complex CP29 from spinach, Nat. Struct. Biol. 18 (2011) 309–316.
[43] T. Morosinotto, M. Ballottari, F. Klimmek, S. Jansson, R. Bassi, The association of the antenna system to Photosystem I in higher plants, J. Biol. Chem. 280 (2005) 31050–31058.
[44] A. Amunts, H. Toporik, A. Borovikova, N. Nelson, Structure determination and improved model of plant Photosystem I, J. Biol. Chem. 285 (2010) 3478–3486.
[45] K.N. Ferreira, T.M. Iverson, K. Maghlaoui, J. Barber, S. Iwata, Architecture of the photosynthetic oxygen-evolving center, Science 19 (2004) 1831–1838.